Contrib Mineral Petrol (2011) 161:845–861
DOI 10.1007/s00410-010-0568-1

ORIGINAL PAPER

Multistage melt/fluid-peridotite interactions in the refertilized lithospheric mantle beneath the North China Craton: constraints from the Li–Sr–Nd isotopic disequilibrium between minerals of peridotite xenoliths

Yan-Jie Tang · Hong-Fu Zhang · Eizo Nakamura · Ji-Feng Ying

Received: 12 March 2010 / Accepted: 4 August 2010 / Published online: 19 August 2010

Abstract Elemental and Li–Sr–Nd isotopic data of minerals in spinel peridotites hosted by Cenozoic basalts allow us to refine the existing models for Li isotopic fractionation in mantle peridotites and constrain the melt/fluid-peridotite interaction in the lithospheric mantle beneath the North China Craton. Highly elevated Li concentrations in cpx (up to 24 ppm) relative to coexisting opx and olivine (<4 ppm) indicate that the peridotites experienced metasomatism by mafic silicate melts and/or fluids. The mineral δ^7Li vary greatly, with olivine (+0.7 to +5.4‰) being isotopically heavier than coexisting opx (−4.4 to −25.9‰) and cpx (−3.3 to −21.4‰) in most samples. The δ^7Li in pyroxenes are considerably lower than the normal mantle values and show negative correlation with their Li abundances, likely due to recent Li ingress attended by diffusive fractionation of Li isotopes. Two exceptional samples have olivine δ^7Li of −3.0 and −7.9‰, indicating the existence of low δ^7Li domains in the mantle, which could be transient and generated by meter-scale diffusion of Li during melt/fluid-peridotite interaction. The ^{143}Nd/^{144}Nd (0.5123–0.5139) and ^{87}Sr/^{86}Sr (0.7018–0.7062) in the pyroxenes also show a large variation, in which the cpx are apparently lower in ^{87}Sr/^{86}Sr and slightly higher in ^{143}Nd/^{144}Nd than coexisting opx, implying an intermineral Sr–Nd isotopic disequilibrium. This is observed more apparently in peridotites having low ^{87}Sr/^{86}Sr and high ^{143}Nd/^{144}Nd ratios than in those with high ^{87}Sr/^{86}Sr and low ^{143}Nd/^{144}Nd, suggesting that a relatively recent interaction existed between an ancient metasomatized lithospheric mantle and asthenospheric melt, which transformed the refractory peridotites with highly radiogenic Sr and unradiogenic Nd isotopic compositions to the fertile lherzolites with unradiogenic Sr and radiogenic Nd isotopic compositions. Therefore, we argue that the lithospheric mantle represented by the peridotites has been heterogeneously refertilized by multistage melt/fluid-peridotite interactions.

Keywords Peridotite xenoliths · Lithium isotope · Melt/fluid-peridotite interaction · Lithospheric mantle · North China Craton

Communicated by T. L. Grove.

Y.-J. Tang (✉) · H.-F. Zhang · J.-F. Ying
State Key Laboratory of Lithospheric Evolution, Institute of Geology and Geophysics, Chinese Academy of Sciences, P.O. Box 9825, 100029 Beijing, China
e-mail: tangyanjie@mail.igcas.ac.cn

E. Nakamura
The Pheasant Memorial Laboratory for Geochemistry and Cosmochemistry, Institute for Study of the Earth's Interior, Okayama University at Misasa, Tottori-ken 682-0193, Japan

Introduction

Lithium element and isotope geochemistry is increasingly being used to trace fluid-related processes (e.g., Huh et al. 1998; Marks et al. 2007; Marschall et al. 2007; Lee et al. 2008; Penniston-Dorland et al. 2010) and geochemical recycling such as the return to the Earth's mantle of crust by subduction (e.g., Tomascak et al. 2000; Kobayashi et al. 2004; Elliott et al. 2006; Agostini et al. 2008; Halama et al. 2008; Košler et al. 2009). The main reason that makes Li a powerful tracer is the great range of δ^7Li from −30 to +50‰ in terrestrial samples (Tomascak 2004; Tang et al. 2007a), which is ascribed to the large relative mass difference between ^{6}Li and ^{7}Li.

Lithium isotope compositions of mantle materials may be affected by diffusion processes due to the exceptionally

high diffusivity of Li (Coogan et al. 2005) and faster diffusion of ^{6}Li than ^{7}Li (Richter et al. 2003). For example, high-temperature diffusive fractionation has been invoked to account for striking δ^{7}Li variations in country rocks of pegmatite (Teng et al. 2006), within individual phenocrysts (Beck et al. 2006; Parkinson et al. 2007) and intragranular, intergranular and intersample scales in mantle-derived rocks (e.g., Lundstrom et al. 2005; Jeffcoate et al. 2007; Kaliwoda et al. 2008; Aulbach and Rudnick 2009).

In a recent study, it is proposed that significant Li isotopic zoning can occur as a natural consequence of cooling magmatic systems (Gallagher and Elliott 2009). This idea is consistent with the suggestion that δ^{7}Li variations in lava-hosted peridotites may be related to different cooling times of flows (Ionov and Seitz 2008), rather than the result of diffusive fractionation related to melt/fluid-rock reaction (e.g., Rudnick and Ionov 2007; Aulbach and Rudnick 2009). Despite major advances in Li isotopic geochemistry, the processes responsible for Li isotope fractionation in mantle peridotites, such as diffusion of Li during melt/fluid-peridotite interactions, are still poorly understood.

This paper reports element and Li–Sr–Nd isotopic data for minerals in peridotite xenoliths from the Hannuoba, Fanshi and Hebi localities in the Trans-North China Orogen of the North China Craton (NCC, Fig. 1). These data, together with previous geological and geochemical evidence, allow us to refine the existing models for Li isotopic fractionation in mantle peridotites and to probe the importance of melt/fluid-peridotite interaction in the evolution of lithospheric mantle beneath the NCC.

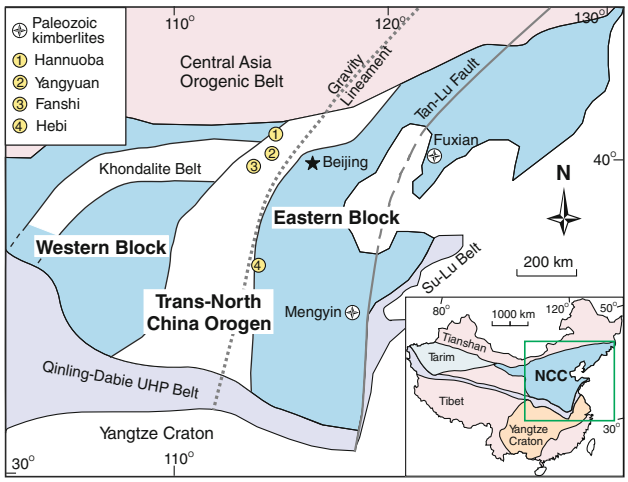

Fig. 1 Simplified geological map showing xenolith localities mentioned in the text and tectonic subdivisions of the North China Craton (*NCC*) (Zhao et al. 2008). The NCC is cut by two major linear zones—Tan-Lu fault zone to the east and south–north gravity lineament to the west. *Inset* shows location of the NCC relative to other blocks and fold belts

Geological setting

The NCC (Fig. 1) is one of the world's oldest cratons, containing Archean crustal remnants as old as 3.8 Ga (Liu et al. 1992). It comprises the Eastern Block, the Western Block and the Trans-North China Orogen, which is an ancient orogen formed by the collision between the Eastern and Western Blocks at *ca* 1.85 Ga, marking the final amalgamation of the NCC (Zhao et al. 2008). The NCC experienced multiple circum-craton subductions and collisions, which are manifested by the Paleozoic to Triassic Qinling–Dabie–Sulu ultrahigh-pressure belt in south, the Central Asian Orogenic Belt in north and the Mesozoic–Cenozoic subduction of Pacific plate in east. These subduction and collision events may have affected the compositions and geophysical characteristics of the lithospheric mantle beneath the NCC (Menzies et al. 2007 and references therein) *and* thus be the key driving force for the transformation of the lithospheric mantle during the Phanerozoic (Zhang et al. 2002, 2003).

Peridotite xenoliths from the Ordovician diamondiferous kimberlites in Mengyin and Fuxian Counties (Fig. 1) represent samples of an ancient mantle lithosphere and indicate a thick (>200 km), cold (geotherm *ca* 40 mW/m^{2}) and refractory lithospheric keel beneath the eastern NCC prior to the Paleozoic (e.g., He 1987; Zhang et al. 1989; Dobbs et al. 1994; Meyer et al. 1994; Chi and Lu 1996). Nevertheless, the mantle xenoliths carried in the Cenozoic basalts reveal that the Cenozoic lithosphere is thin (<80 km), hot (geotherm *ca* 80 mW/m^{2}) and of fertile composition (e.g., Song and Frey 1989; Fan and Menzies 1992; Tatsumoto et al. 1992; Xu et al. 1998a; Fan et al. 2000; Xu 2001; Zheng et al. 2001). These observations suggest that >100 km of ancient cratonic lithosphere beneath the eastern NCC was lost during the Phanerozoic (e.g., Griffin et al. 1992; Menzies et al. 1993).

Sample description

The samples are spinel-facies peridotite xenoliths from the Hannuoba (*ca* 22 Ma, northern margin of the craton), Fanshi (*ca* 25 Ma, northern part of the craton) and Hebi (*ca* 4 Ma, central part of the craton) Cenozoic basalts (Fig. 1). The Hannuoba peridotites gave a Re–Os isochron age of *ca* 1.9 Ga (Gao et al. 2002) and have Re depletion ages as old as 2.2 Ga (Zheng et al. 2007; Xu et al. 2008a; Zhang et al. 2009). When compared to worldwide cratonic peridotites, these peridotites have high Al_2O_3 content of cpx and opx, relatively low Mg# of olivine and Cr# of spinel (Fig. 2). These compositions are thus markedly different from cratonic mantle lithosphere found beneath other Archean cratons (Rudnick et al. 2004). It has been suggested that

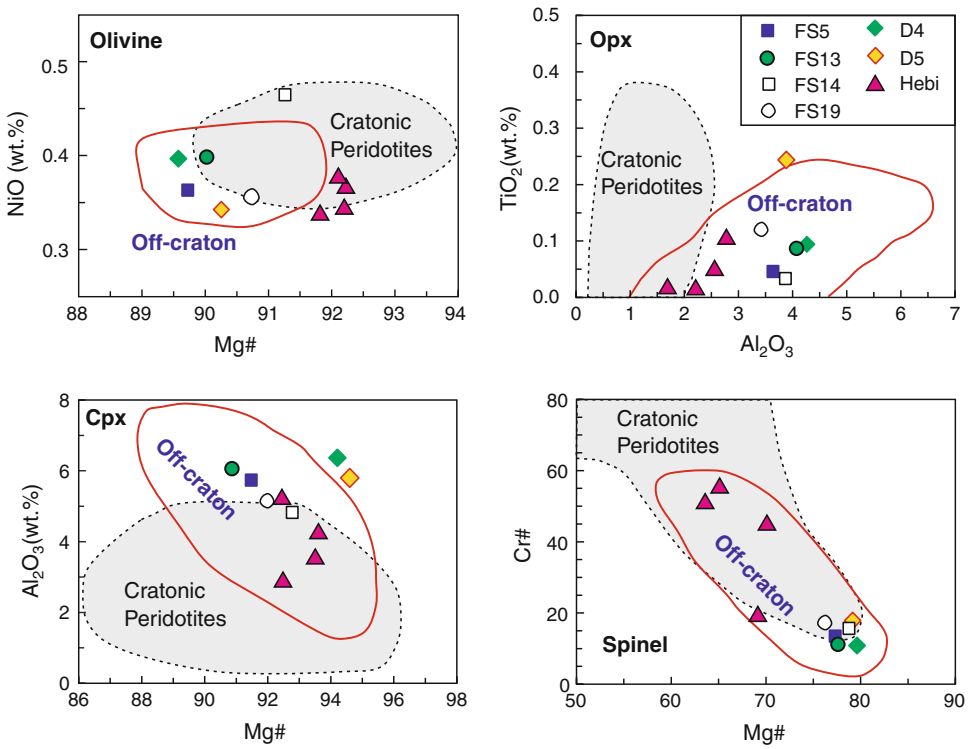

Fig. 2 Mineral compositions for the peridotites. Fields for worldwide off-craton spinel peridotites and cratonic peridotites, including Kaapvaal, east Greenland, Siberia and Tanzania, are from Rudnick et al. (2004)

trace element and Sr–Nd–Os–Li–Fe isotopic compositions of the Hannuoba peridotites reflect considerably recent mantle metasomatic overprinting (Song and Frey 1989; Rudnick et al. 2004; Tang et al. 2007b; Xu et al. 2008a; Zhang et al. 2009; Zhao et al. 2010).

Detailed petrographic descriptions for the Hannuoba samples D4 and D5 have been reported (Tang et al. 2007b). Sample D4 has a porphyroclastic texture. Most olivine and opx grains are *ca* 1–2 mm in diameter with a few up to 3 mm, and large olivine grains are usually kink-banded, indicative of high-temperature plastic deformation (Herzberg 1993). Cpx grains are less than 1 mm in diameter. Sample D5 is coarse-grained and shows coarse-granular and porphyroblastic texture, with mineral mode similar to that of sample D4. Olivine grains are 2–3 mm in diameter with a few grains up to 5 mm. Opx grains are 3–4 mm and cpx *ca* 1 mm.

The Fanshi peridotite xenoliths have Paleoproterozoic Re depletion ages (Xu et al. 2008b). Four lherzolite samples, FS5, FS13, FS14 and FS19, are selected here. These are broadly rounded and range from 5 to 7 cm across. The FS14 is coarse to medium-grained and has porphyroblastic texture. It is relatively poor in modal cpx (8%), similar to the harzburgite xenoliths (cpx < 5%) at this locality (Tang et al. 2008). Samples FS5, FS13 and FS19 are medium to fine grained and have equilibrated textures. Most olivine and opx grains in these samples are 1–2 mm in diameter, and their cpx grains are less than 1 mm in diameter. Cpx modes exceed 10%. The mineral compositions are fertile, similar to those of the "oceanic" lithospheric mantle in eastern China (Fan et al. 2000; Zhang et al. 2007).

Four Hebi samples HB27, HB30, HB80 and HB81 selected here are coarse-granular harzburgites [olivine: 70–79% (Fo = 91.9–92.3%); opx: 19–25%; cpx: <2%; and trace amounts of spinel; Appendix Table]. They are characterized by high Fo in olivine and interpreted as the relics of old lithospheric mantle (Zheng et al. 2001) with Archean Re depletion ages (as old as 3.0 Ga; Zheng et al. 2007). Compared to Archean lithospheric mantle peridotites (Fo > 92.5), relatively lower Fo values of these harzburgites imply that the old lithospheric mantle has been modified through peridotite–melt interaction, which can transform a major element-depleted peridotite into relatively fertile one (Zhang 2005).

Analytical methods

Major element compositions of minerals were determined with a Cameca SX51 electron probe micro-analyzer at the Institute of Geology and Geophysics, Chinese Academy of Sciences. Trace element and Sr–Nd–Li isotope analyses were carried out at the Pheasant Memorial Laboratory (PML) for Geochemistry and Cosmochemistry, Institute for Study of the Earth's Interior, Okayama University at Misasa, Japan.

Fresh xenoliths, without any weathering features by thin section observation, were crushed and sieved with stainless

steel sieves (180–250 μm). Olivine, opx and cpx separates were handpicked under a binocular microscope and cleaned in an ultrasonic bath in deionized water for 15 min. The separates then were leached by HCl as shown in Tang et al. (2007a). After drying at 110°C, the mineral separates were ground into powders using a silicon nitride mortar.

Trace element analyses of cpx, including Li in olivine and opx, followed the procedures of Moriguti et al. (2004) and Makishima and Nakamura (2006) using an Agilent 7500cs quadrupole ICP mass spectrometer. The analytical reproducibility was <5% (RSD).

The Li chemical separation and isotope analyses by a Neptune MC-ICP-MS have been reported (Moriguti and Nakamura 1998; Tomascak et al. 1999; Tang et al. 2007b). Analytical uncertainty was <0.06‰ (2σ mean). The difference between the δ^7Li of the two L-SVEC standards bracketing each sample was typically <0.4‰ and averaged *ca* 0.2‰. During the course of this study, obtained δ^7Li value of standard rock sample, GSJ JB-2, was 5.0 ± 0.5‰ (2σ, $n = 5$), consistent with values published previously within analytical error (+4.9±0.7‰ 2σ reproducibility, Moriguti and Nakamura 1998; 5.1 ± 1.1‰, Tomascak et al. 1999; 4.7 ± 0.3‰, Magna et al. 2008; 4.7 ± 1.3‰, Halama et al. 2009).

The Sr and Nd isotopic compositions of cpx and opx separates were measured using a Finnigan MAT-262 thermal ionization mass spectrometer following the methods described in Yoshikawa and Nakamura (1993) and Nakamura et al. (2003). The mineral powders were weighed (10–40 mg for cpx and 100–400 mg for opx). Replicate analyses yielded $^{87}Sr/^{86}Sr$ of 0.710279 ± 0.000023 (2σ, $n = 10$) for the NBS 987 and $^{143}Nd/^{144}Nd$ of 0.511738 ± 0.000012 (2σ, $n = 10$) for in-house standard, PML Nd, which corresponds to $^{143}Nd/^{144}Nd = 0.5118740$ of La Jolla standard. The total procedural blanks are 4, 22, 1 and 7 pg for Rb, Sr, Sm and Nd, respectively.

Analytical results

Major and trace elemental compositions

The minerals (olivine, opx and cpx) are homogeneous in major oxides based on analyses from core to rim. The average composition is reported in Table 1. The forsterite contents (Fo) or Mg# range from 89.6 to 92.3, and most of them are significantly lower than those of typical Archean lithospheric mantle (Fo > 92.5; Boyd 1989). The Hebi harzburgites have higher Fo (~92) than the Fanshi and Hannuoba (90–91), and most of them plot in the fields for cratonic peridotites. However, the minerals compositions for the Fanshi and Hannuoba lherzolites are generally similar to those of global off-craton spinel peridotites and different from those of typical old cratonic peridotites (Fig. 2; Rudnick et al. 2004). Some peridotite xenoliths from this region have SiO_2 contents higher than the primitive mantle (Fig. 3) and cannot be the residue of melt extraction.

The cpx show a large variation in chondrite-normalized rare earth element (REE) patterns from light REE (LREE)-depleted to LREE-enriched profiles (Fig. 4). Most Hebi and Fanshi samples have relatively high LREE contents and positive primitive mantle-normalized Li anomaly, whereas the Hannuoba samples show lower LREE contents and Li depletion (Table 2; Fig. 4). Some of the Fanshi samples have heavy-REE (HREE) contents higher than the Hannuoba and Hebi samples. Two samples from the Hebi (HB27 and HB30) show very low HREE and are characterized by a prominent trough from Gd to Tm, showing at least a two-stage feature of a partial melting followed by mantle metasomatism. In addition, the cpx display Rb and Ba depletion but weak enrichment of Sr.

Li contents in the coexisting minerals vary greatly (Table 3; Fig. 5). The Fanshi cpx are the highest in Li contents (13–24 ppm), followed by opx (4–7 ppm) and olivine (2–4 ppm). Compared with the Fanshi peridotites, the Hannuoba samples are lower in Li contents in cpx (2.4–2.7 ppm), opx (1.4–1.9 ppm) and olivine (1.4–1.5 ppm). For the Hebi harzburgites, Li contents in olivine (1–2 ppm) are similar to the normal mantle, but those in opx (4–8 ppm) and cpx (7–13 ppm) are apparently higher than the normal mantle (Fig. 5).

Sr, Nd and Li isotope ratios of mineral separates

Sr and Nd isotopic compositions of cpx and opx separates show a large variation (Table 4), ranging from depleted mantle (DM) to enriched mantle (EM1)-like Sr–Nd isotopic characteristics (Fig. 6), which are consistent with those documented in the previous investigations (Rudnick et al. 2004; Tang et al. 2008). The cpx in most peridotites are lower in $^{87}Sr/^{86}Sr$ and higher in $^{143}Nd/^{144}Nd$ than coexisting opx (Fig. 6). The peridotites with strongly different Sr–Nd isotopic compositions between cpx and opx are lower in $^{87}Sr/^{86}Sr$ (0.7018–0.7034) and higher in $^{143}Nd/^{144}Nd$ (0.5131–0.5139) than those whose Sr–Nd isotope compositions in cpx and opx are closer (Table 4).

Li isotopic compositions of the mineral separates show extremely large variations, with δ^7Li ranging from +5.4 to −7.9‰ in olivine, −4.4 to −26‰ in opx and −3.3 to −21‰ in cpx (Table 3). For most of the samples, olivine has higher δ^7Li (>+0.7‰) than coexisting opx and cpx (<−10‰). In sample FS5, olivine has δ^7Li of −7.9‰, which is isotopically lighter than the coexisting opx (−5.3‰), but heavier than the coexisting cpx (−8.4‰). Remarkable fractionations of Li isotopes between coexisting minerals are observed. The maximum between pyroxenes and olivines is 27‰ (Table 3).

Table 1 Major element composition (wt%) of minerals in the peridotites (average value of *n* analyses)

Sample	FS5				FS13				FS14				FS19				D4			
Rock	Sp-lherzolite				Sp-lherzolite				Sp-lherzolite				Sp-lherzolite				Sp-lherzolite			
Mineral	Ol	Cpx	Opx	Sp	Ol	Cpx	Opx	Sp	Ol	Cpx	Opx	Sp	Ol	Cpx	Opx	Sp	Ol	Cpx	Opx	Sp
Point (*n*)	4	5	6	4	4	4	5	5	5	5	6	4	4	6	6	4	4	4	4	2
SiO_2	41.24	52.64	55.22		40.87	51.82	55.53		41.89	53.69	56.98		41.49	53.09	55.63		41.00	52.09	55.36	
TiO_2		0.45	0.04	0.10		0.6	0.09	0.15		0.24	0.04	0.11		0.40	0.12	0.14		0.52	0.10	0.07
Al_2O_3		5.74	3.67	53.63		6.07	4.1	57		4.82	3.87	52.53		5.18	3.42	50.00		6.55	4.25	58.34
Cr_2O_3		0.94	0.28	13.06		0.78	0.34	11.79		0.78	0.37	15.55		1.01	0.34	16.78		0.79	0.33	9.53
FeO	10.00	2.58	6.28	10.44	9.97	2.64	6.15	10.7	8.57	2.25	5.35	9.76	9.05	2.47	5.82	11.29	10.08	1.64	6.58	9.43
MnO	0.14	0.05	0.10	0.09	0.12	0.1	0.16	0.11	0.13	0.02	0.13	0.08	0.15	0.10	0.15	0.10	0.09	0.09	0.14	0.09
MgO	48.51	15.51	33.02	20.21	49.71	15.61	33.85	20.43	49.83	16.02	33.47	20.54	49.37	15.67	33.36	19.89	48.01	14.92	32.54	20.29
CaO	0.06	19.28	0.60		0.08	20.77	0.58		0.07	20.08	0.70		0.03	20.55	0.64		0.06	20.49	0.57	
Na_2O		1.39	0.08			1.57	0.09			1.25	0.08			1.39	0.09			1.76	0.09	
NiO	0.36		0.00	0.29	0.39		0.03	0.36	0.47		0.06	0.40	0.36		0.17	0.23	0.40		0.05	0.40
Total	100.3	98.6	99.3	97.8	101.1	100.0	100.9	100.5	101.0	99.1	101.0	99.0	100.4	99.9	99.7	98.4	99.6	98.9	100.0	98.2
Mg#	89.7	91.5	90.4	77.7	90.0	91.4	90.8	77.5	91.3	92.8	91.8	79.1	90.8	92.0	91.2	76.0	89.6	94.3	89.9	79.5
Cr#				14.2				12.3				16.8				18.6				10.0
Sample	D5				HB27				HB30				HB80				HB81			
Rock	Sp-lherzolite				Sp-harzburgite				Sp-harzburgite				Sp-harzburgite				Sp-harzburgite			
Mineral	Ol	Cpx	Opx	Sp	Ol	Cpx	Opx	Sp	Ol	Cpx	Opx	Sp	Ol	Cpx	Opx	Sp	Ol	Cpx	Opx	Sp
Point (*n*)	4	4	4	2	5	6	5	4	6	6	6	4	6	6	6	4	5	5	5	4
SiO_2	41.34	52.62	55.59		40.32	52.38	55.1		40.87	52.9	56.02		40.8	53.39	56.83		40.16	53.52	57.52	
TiO_2		0.26	0.36	0.07		0.03	0.12	0.31		0.22	0.04	0.04		0.02	0.01	0.07		0.08	0.01	0.32
Al_2O_3		5.81	3.69	52.46		4.16	2.98	25.03		5.38	2.86	29.23		3.45	2.46	23.9		2.43	1.76	25.44
Cr_2O_3		1.12	0.34	15.71		1.06	0.92	40.62		1.85	0.7	36.22		1.29	0.79	42.22		2.3	0.63	41.98
FeO	9.52	1.57	5.69	9.45	7.55	2.11	4.19	14.36	7.99	2.31	4.95	13.77	7.78	2.28	4.85	15.15	7.82	2.41	4.96	15.96
MnO	0.10	0.13	0.16	0.07	0.12	0.09	0.11	0.02	0.09	0.08	0.1	0.1	0.12	0.06	0.11	0.02	0.1	0.06	0.13	0.02
MgO	48.97	15.08	32.91	19.67	50.2	17.17	34.2	16.86	50.62	15.99	33.8	18.22	50.8	17.88	34.31	15.88	50.83	16.48	34.68	15.71
CaO	0.04	20.67	0.47		0.07	20.31	0.78		0.05	18.59	0.81		0.09	20.6	0.77		0.05	21.09	0.6	
Na_2O		1.73	0.07			0.91	0.04			1.61	0.21			0.52	0.04			0.92	0.08	
NiO	0.34		0.11	0.34	0.36		0.09	0.22	0.33	0	0.15	0.23	0.34		0.1	0.24	0.37		0.1	0.18
Total	100.4	99.0	99.4	97.8	98.7	98.3	98.5	97.5	100.0	99.0	99.6	97.8	100.0	99.6	100.3	97.5	99.4	99.3	100.5	99.6
Mg#	90.3	94.5	91.2	78.9	92.3	93.6	93.6	67.9	91.9	92.6	92.5	70.4	92.2	93.4	92.7	65.4	92.1	92.5	92.6	63.9
Cr#				16.9				52.5				45.7				54.6				52.9

Major element composition (wt%) of minerals in the peridotites (average value of *n* points)

Ol olivine, *opx* orthopyroxene, *cpx* clinopyroxene, *sp* spinel, Mg# = 100 × molar Mg/(Mg + Fe), Cr# = 100 × molar Cr/(Cr + Al). Blank is below detection limit. Data for D4 and D5 are from Tang et al. (2007a)

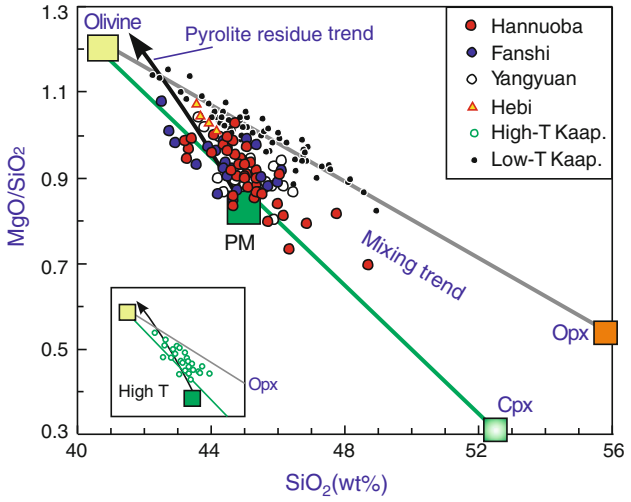

Fig. 3 MgO/SiO_2 versus SiO_2 (wt%) showing peridotites from the North China Craton relative to the residue trend for pyrolite and to mixing trends between olivine and opx (Walter 1998) and between olivine and cpx. Data sources for the Chinese peridotites: Fan and Hooper (1989), Song and Frey (1989), Chen et al. (2001), Rudnick et al. (2004), Ma and Xu (2006), Tang et al. (2008), Xu et al. (2008b) and this study. High-temperature and low-temperature peridotites from Kaapvaal, southern Africa and fields for olivine and opx are taken from Walter (1998). Field for cpx represents the average composition of cpx in Hannuoba peridotites and primitive mantle (*PM*) taken from McDonough and Sun (1995)

Discussion

Elemental geochemistry

Mafic melt extraction from a fertile peridotite will form a relatively refractory lherzolite or harzburgite (Kushiro 2001). Thus, the residue is variously depleted in basaltic components such as Al, Ca, Ti and Na. A typical feature of Archean mantle is the presence of highly refractory harzburgites and cpx-poor lherzolites (Boyd 1989). Inversely, many xenoliths and xenocrysts data suggest that the lithospheric mantle beneath Archean/Proterozoic areas has been extensively refertilized by metasomatic processes, with the addition of melts rich in basaltic components (including Al, Ca and Fe) to originally depleted peridotites (Griffin et al. 2003; Carlson et al. 2004; Simon et al. 2007; references therein). Most of the Fanshi and Hannuoba samples are plotted in the field for off-craton peridotites due to their relatively fertile mineral compositions (Fig. 2) and lower Fo of olivines (<91.5) than typical old cratonic peridotites (>92) although the NCC is an Archean craton. This indicates different-extent refertilization of the old lithospheric mantle beneath the NCC by melt addition (Tang et al. 2008; Zhang et al. 2009, 2010), by which some peridotites are relatively fertile in mineral compositions and thus bear a resemblance to the newly accreted lithospheric mantle (Fan et al. 2000). Most of the Hebi harzburgites dropped in the fields for global cratonic peridotites due to their high Mg# in olivine and cpx, and high Cr# in spinel, and thus they were interpreted as the relics of old lithospheric mantle (Zheng et al. 2001, 2007). Compared to Archean lithospheric mantle peridotites (Fo > 92.5), relatively lower Fo values and higher Al_2O_3 contents (Fig. 2) of these harzburgites imply that the Archean lithospheric mantle has been refertilized by melt addition. In contrast, the Hebi samples experienced less-degree refertilization than the others, which is also evidenced in Fig. 3, showing the correlation of MgO/SiO_2 ratio with SiO_2 in cratonic peridotites from the North China Craton and the Kaapvaal craton, southern Africa. Compositions of the low-temperature peridotite

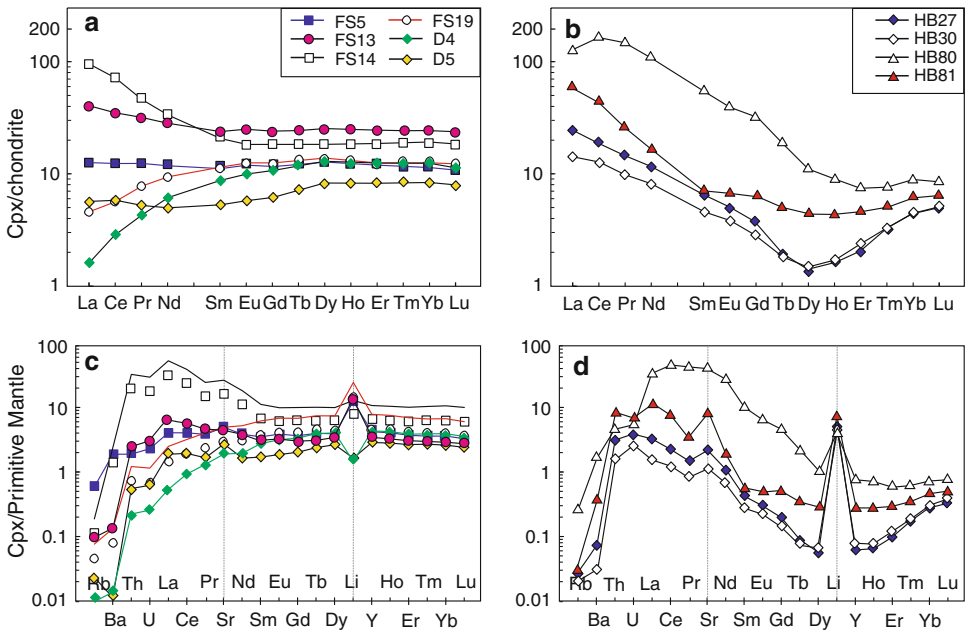

Fig. 4 Chondrite-normalized REE patterns (**a**, **b**) and primitive mantle-normalized spidergram (**c**, **d**) for cpx from the Hannuoba, Fanshi and Hebi peridotites. Normalization values: chondrite (Anders and Grevesse 1989), primitive mantle (McDonough and Sun 1995)

Table 2 Trace element compositions (ppm) of cpx

Sample	FS5	FS13	FS14	FS19	HB27	H30	HB80	HB81	D4	D5
Rb	0.385	0.062	0.072	0.029	0.014	0.013	0.181	0.019	0.006	0.015
Ba	13.6	0.898	10.3	0.563	0.525	0.207	13.5	2.65	0.098	0.080
Th	0.167	0.207	1.73	0.063	0.270	0.153	0.434	0.815	0.019	0.049
U	0.050	0.064	0.386	0.015	0.080	0.055	0.121	0.149	0.006	0.014
La	2.90	4.85	22.7	1.06	2.39	1.06	26.0	8.86	0.382	1.34
Ce	7.49	10.3	43.1	3.49	4.29	2.24	98.7	14.3	1.71	3.57
Pb	0.328	0.466	2.57	0.354	0.174	0.138	1.07	0.090	0.049	0.060
Pr	1.10	1.31	4.19	0.684	0.429	0.242	12.4	1.03	0.374	0.475
Sr	108	116	348	64.4	57.4	25.6	994	211	41.5	59.6
Nd	5.41	5.68	15.3	4.36	1.61	0.97	42.9	2.64	2.74	2.31
Sm	1.62	1.42	3.07	1.70	0.214	0.128	4.78	0.252	1.28	0.783
Eu	0.675	0.584	1.03	0.709	0.059	0.039	1.16	0.083	0.551	0.325
Gd	2.26	1.92	3.69	2.51	0.136	0.087	3.05	0.308	2.08	1.25
Tb	0.447	0.368	0.674	0.495	0.009	0.009	0.258	0.039	0.441	0.268
Dy	3.00	2.54	4.55	3.37	0.039	0.042	0.799	0.212	3.1	2.03
Y	20.0	17.0	30.2	22.1	0.304	0.336	3.71	1.45	20.5	13.6
Ho	0.692	0.573	1.06	0.763	0.011	0.012	0.133	0.046	0.722	0.478
Er	1.85	1.58	3.00.	2.06	0.047	0.059	0.287	0.142	1.93	1.33
Tm	0.276	0.246	0.475	0.304	0.014	0.014	0.048	0.026	0.300	0.207
Yb	1.85	1.60	3.24	2.04	0.150	0.149	0.390	0.238	2.02	1.34
Lu	0.253	0.223	0.459	0.275	0.027	0.029	0.062	0.039	0.271	0.185
ΣREE	29.8	33.2	106	23.8	4.8	5.1	191	28.2	17.9	15.9
$(La/Yb)_N$	1.08	2.10	4.85	0.36	10.10	4.92	46.10	25.7	0.13	0.69

Data for D4 and D5 are from Tang et al. (2007a)

Table 3 Li concentrations and isotopic compositions of mineral separates in the peridotites

Sample	Olivine			Opx			Cpx		
	Li (ppm)	δ^7Li	2σ	Li (ppm)	δ^7Li	2σ	Li (ppm)	δ^7Li	2σ
FS5	3.88	−7.89	0.04	4.73	−5.29	0.03	20.8	−8.43	0.03
FS13	2.06	−2.96	0.04	5.09	−16.45	0.04	23.55	−11.55	0.04
FS14	1.87	1.20	0.04	3.78	−15.41	0.05	12.7	−19.69	0.03
FS19	1.87	3.38	0.04	6.60	−23.47	0.04	24.2	−17.38	0.05
HB27	1.40	0.72	0.05	4.48	−20.19	0.03	7.3	−18.21	0.02
HB30	1.41	2.91	0.04	4.79	−23.20	0.06	7.0	−20.29	0.03
HB80	2.29	0.70	0.04	7.71	−25.98	0.03	7.9	−11.40	0.04
HB81	0.98	0.21	0.04	7.96	−23.71	0.03	13.1	−21.41	0.03
D4	1.51	5.35	0.04	1.37	−5.27	0.05	2.41	−3.25	0.06
D5	1.37	5.20	0.04	1.89	−4.35	0.05	2.72	−7.54	0.05

Data for D4 and D5 are from Tang et al. (2007a)

xenoliths from Kaapvaal show mixing trends between olivine and opx (Walter 1998), while the peridotites from the North China Craton have the compositions displaying mixing trend between olivine and cpx (Fig. 3). This possibly reflects the introduction of cpx into the peridotites during melt metasomatic events, similar to that recognized by Simon et al. (2007).

The variation of cpx REE patterns (Fig. 4) may reflect the effect of melt/fluid-peridotite interaction. LREE enrichments in some cpx (e.g., HB80, FS13 and FS14) indicate mantle metasomatism. Chromatographic migration of LREE-enriched melts through LREE-depleted peridotites is an efficient mechanism (Navon and Stolper 1987). This type of melt–rock interaction produces REE patterns

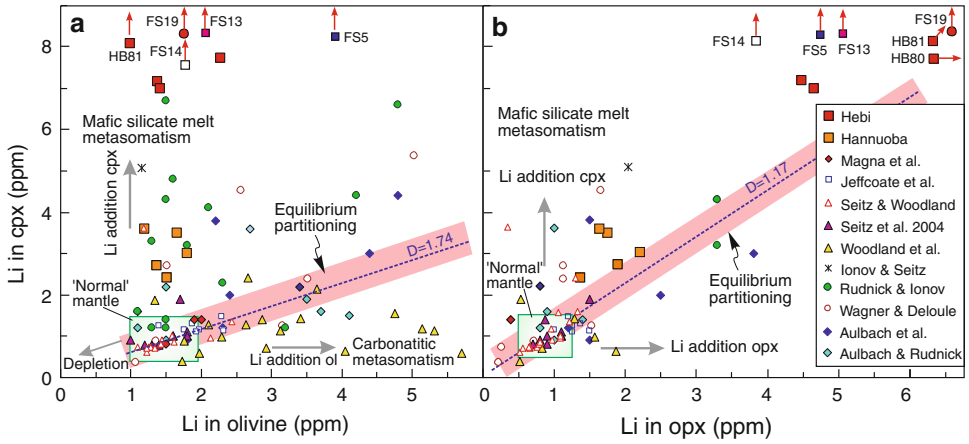

Fig. 5 Li abundance in cpx versus coexisting **a** olivine and **b** opx. Field for 'normal' mantle is represented by fertile to moderately depleted peridotites (Seitz and Woodland 2000). The dashed field represents equilibrium partitioning of Li between minerals based on the new partition coefficients $D^{ol/cpx} = 1.74$ and $D^{cpx/opx} = 1.17$ (Ottolini et al. 2009). *Inset* shows extend diagrams including samples with extremely high Li contents in minerals. Higher Li contents are ascribed to Li ingress by mafic silicate melt metasomatism or/and carbonatitic metasomatism (Seitz and Woodland 2000). Three Hannuoba samples plotted are from Tang et al. (2007a). Data shown for comparison are from the literature (Seitz and Woodland 2000; Seitz et al. 2004; Woodland et al. 2004; Magna et al. 2006; Jeffcoate et al. 2007; Rudnick and Ionov 2007; Wagner and Deloule 2007; Aulbach et al. 2008; Ionov and Seitz 2008; Aulbach and Rudnick 2009)

Table 4 Sr and Nd isotopic compositions for cpx and opx separates in the peridotites

Sample	Weight (mg)	Rb (ppm)	Sr (ppm)	Sm (ppm)	Nd (ppm)	$^{143}Nd/^{144}Nd$	2σ	$^{87}Sr/^{86}Sr$	2σ
Cpx									
D4	43.50	0.005	41.7	1.35	2.73	0.513890	5	0.701770	6
D5	41.51	0.007	57.0	0.78	2.25	0.513159	5	0.702998	7
FS5	10.85	0.362	107	1.79	5.61	0.512762	4	0.704241	6
FS14	11.10	0.051	353	3.24	15.7	0.512270	5	0.706138	5
FS19	13.09	0.021	64.8	1.84	4.44	0.513292	4	0.702102	6
Opx									
D4	403.04	0.002	0.147	0.013	0.016	0.513849	31	0.702203	6
D5	314.89	0.001	0.121	0.006	0.010	0.513105	28	0.703357	7
FS5	68.37	0.347	2.19	0.041	0.125	0.512792	10	0.704314	6
FS14	103.16	0.145	2.28	0.040	0.122	0.512306	5	0.706166	6
FS19	97.52	0.147	0.602	0.035	0.066	0.513202	16	0.703133	5

with extremely variable LREE enrichment, which is typical of that observed in the FS5, D5, HB27 and HB30 (Fig. 4). Although the LREE depletions in D4 and FS19 show a partial melting process, they are the likely consequence that the cpx reach approximate equilibrium with LREE-depleted melts as documented by Xu et al. (1998b) because of their high FeO and TiO_2 contents (Table 2; Fig. 2). The variation observed for the HREE contents likely reflects the variable degrees of partial melting. The positive anomalies of Sr and Li (Fig. 4) may be due to later enrichments related with small-volume melts as described by Bodinier et al. (2004) or fluid-induced overprinting of the mantle (Halama et al. 2009). The negative Li anomaly in Hannuoba peridotites D4 and D5 may reflect (1) the preference of olivine to incorporate Li relative to REE (Tang et al. 2007a) and (2) these peridotites approached equilibrium with LREE-depleted melt/fluid and their Li abundances are close to the normal mantle values.

The Li compositional ranges in olivine and pyroxenes in the normal mantle are 1–1.8 and 0.5–1.3 ppm, respectively (Seitz et al. 2004; Woodland et al. 2004; Jeffcoate et al. 2007). According to the Li partition coefficients of $D^{ol/cpx} = 1.74$ and $D^{cpx/opx} = 1.17$ (Ottolini et al. 2009), Li partitioning in equilibrated peridotites is olivine > cpx > opx. However, Li partitioning observed in peridotites from this study deviates strongly from such an equilibrium trend (Fig. 5). Based on an empirical observation, the preferential Li enrichment in cpx relative to olivine, similar to that of peridotites from Finero, Italy (Seitz and Woodland 2000), far-east Russia (Rudnick and Ionov 2007), French

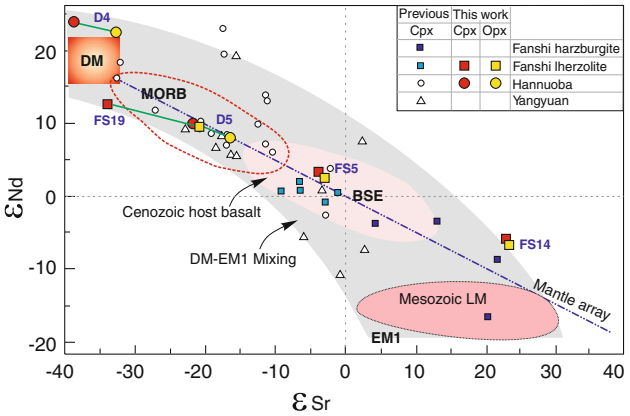

Fig. 6 Variation of ε_{Sr} and ε_{Nd} for cpx and opx in the studied peridotites, together with the published data for peridotite xenoliths (Song and Frey 1989; Tatsumoto et al. 1992; Fan et al. 2000; Rudnick et al. 2004; Ma and Xu 2006; Tang et al. 2008), Cenozoic Fanshi basalts (Tang et al. 2006) from the studied region and for the Mesozoic lithospheric mantle (*LM*) beneath the Trans-North China Orogen (Zhang et al. 2004; Wang et al. 2006). These data are calculated back to 20 Ma when the host basalts erupted. DM, MORB, BSE and EM1 end members are from Zindler and Hart (1986). The analytical uncertainties for the data are less than the symbols. The values used for today's $(^{87}Rb/^{86}Sr)_{BSE}$, $(^{87}Sr/^{86}Sr)_{BSE}$, $(^{147}Sm/^{144}Nd)_{BSE}$, and $(^{143}Ndb/^{144}Ndr)_{BSE}$ are 0.0847, 0.7045, 0.1967 and 0.512638, respectively. The field roughly drawn denotes the DM-EM1 mixing trend

Massif Central (Wagner and Deloule 2007) and Tanzanian Labait volcano (Aulbach et al. 2008), indicates that these peridotites could have been affected by the infiltration of mafic silicate melt. Nevertheless, from available cpx-fluid experimental partitioning data (Brenan et al. 1998), it cannot be ruled out that the metasomatizing agent was a fluid. The preferential Li enrichment in cpx relative to opx (Fig. 5) suggests that the cpx are more susceptible to the melt/fluid infiltration than coexisting opx and olivine due to faster diffusion of Li in cpx than in olivine (Dohmen et al. 2010).

Sr–Nd isotopic characteristics and melt–peridotite interaction

The linear trend on Sr–Nd isotope diagrams for mantle-derived rocks from the DM end member to and beyond BSE (Fig. 6), known as "mantle array", was traditionally explained by metasomatism of ancient melting residues by asthenospheric and other components enriched in incompatible elements (e.g., Menzies and Murthy 1980). Thus, the radiogenic Sr and unradiogenic Nd isotopic compositions in the Fanshi and Yangyuan peridotites reflect ancient enrichment processes of the subcontinental lithospheric mantle, as previously documented for xenoliths from this region (Ma and Xu 2006; Tang et al. 2008; Xu et al. 2008b). Large variation in the Sr–Nd isotopic ratios of cpx (Fig. 6), from DM to EM1-like signature, indicates that the lithospheric mantle reflected by these peridotites could have been previously modified by melts/fluids that increased the Rb/Sr and decreased Sm/Nd ratios in the old lithosphere and then experienced a secular evolution (Wang et al. 2006; Tang et al. 2008). The ancient enrichment event was suggested to have been closely related with the Paleoproterozoic subduction/collision between the Eastern Block and the Western Block of the NCC occurred at *ca* 1.85 Ga (Wang et al. 2006; Zhao et al. 2008).

Unradiogenic Sr and radiogenic Nd isotopic compositions in the Hannuoba and FS19 lherzolites (Fig. 6) could be the products of recent asthenospheric melt–peridotite interaction (Tang et al. 2008; Zhang et al. 2009), i.e., old lithospheric mantle with highly radiogenic Sr and unradiogenic Nd isotopic compositions refertilized by the addition of asthenospheric melt. Because the melt derived from the asthenosphere is low in $^{87}Sr/^{86}Sr$ and high in $^{143}Nd/^{144}Nd$ ratios, the products should be low in $^{87}Sr/^{86}Sr$ and high in $^{143}Nd/^{144}Nd$ relative to their precursors from the old lithosphere having radiogenic Sr isotopic ratios (Zhang et al. 2004). Further evidence for the melt–peridotite interaction is that some peridotite xenoliths from the region (including Hannuoba, Yangyuan and Fanshi localities) have Sr–Nd isotopic compositions that plot to the right of the "mantle array" (Fig. 6) because the decoupling of Sr and Nd isotopes in some peridotites could be due to "chromatographic" effects of melt percolation as indicated by numeric modeling (Ionov et al. 2002). Moreover, the samples D4, D5 and FS19 are higher in ε_{Nd} and lower in ε_{Sr} than FS5 and FS14, indicating that the former experienced higher degrees of interaction with the asthenospheric melts than the latter. This is consistent with their depleted REE patterns $(La/Yb)_N < 1$ (Table 2) because the elemental and isotopic patterns of the mineral could have been partly or totally reset upon interaction of peridotites with asthenospheric melts.

The difference in Sr and Nd isotope compositions between the coexisting cpx and opx may reflect isotopic disequilibrium. In order to cover a wide time span, we correct the Sr and Nd isotope ratios back to the time of 20, 200 Ma and 2 Ga, respectively (Fig. 7). The apparent difference in the isotope compositions between cpx and opx can be still observed at each time. If the formation age of the peridotites is assumed to be 2 Ga, the isotope difference between cpx and opx is very large. Therefore, the Sr–Nd isotopic differences between cpx–opx pairs cannot be explained by radiogenic ingrowth since the peridotites formed, and thus represent intermineral isotopic disequilibrium caused by later processes.

Intermineral isotopic disequilibrium in some mantle peridotite, for example, Sr isotopic differences between coexisting minerals like cpx and opx or cpx and olivine, has been observed in early studies of mantle xenoliths (e.g., Paul 1971; Burwell 1975; Jagoutz 1988). In most cases,

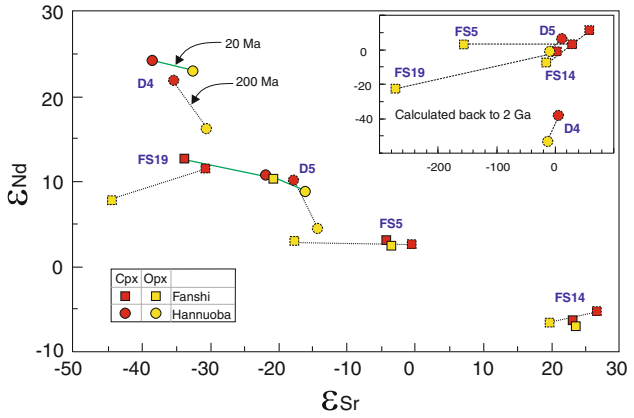

Fig. 7 ε_{Sr} versus ε_{Nd} diagram for the cpx and opx in the studied peridotites. The shown data are calculated back to the time of 2 Ga, 200 and 20 Ma. Normalized $^{87}Sr/^{86}Sr$ and $^{143}Nd/^{144}Nd$ values are 0.7045 and 0.512638, respectively

coexisting phases were found to be in Nd isotopic equilibrium, but opx and olivine showed more radiogenic Sr than coexisting cpx. This phenomenon was ascribed to late-stage contamination, i.e., the data for low Sr concentration phases (opx or olivine) are biased toward values for ubiquitous contaminants, either on grain boundaries or associated with fluid inclusions, unless extreme care is taken to obtain minerals of high optical purity (Jagoutz et al. 1980; Menzies and Murthy 1978; Stosch et al. 1986; Zindler and Jagoutz 1988). For example, Jagoutz et al. (1980) found that opx and cpx were in Nd isotopic equilibrium although the Sr isotope ratio of opx (0.7036) was significantly higher than that in the cpx (0.7023) in a spinel lherzolite from Kilbourne Hole. The authors considered that the higher $^{87}Sr/^{86}Sr$ in the opx was likely the result of secondary contamination, which had not been totally removed during sample preparation.

However, both Sr and Nd isotopic disequilibria between coexistent phases in some mantle peridotites were recognized and attributed to recent mantle metasomatic component addition or redistribution without re-equilibration (Richardson et al. 1985; McDonough and McCulloch 1987; Jagoutz 1988). Even reaction with enclosing magma in the case of xenoliths may result in the different isotopic compositions in constituent minerals of peridotites (Basu and Murthy 1976; Zindler and Jagoutz 1988). There are two possible scenarios for the isotopic disequilibrium: (1) all minerals had the same isotopic composition before the late metasomatic event, which may have involved introduction of a melt/liquid that equilibrated with the outermost parts of minerals; (2) isotopic equilibration could occur within given "domains" (possibly in some minerals prior to the metasomatism) of the peridotite but may not have occurred between "domains", i.e., incomplete equilibration or local resetting of isotopes during the mantle metasomatism (Jagoutz 1988).

In this study, the Sr and Nd isotopic disequilibria between coexisting cpx and opx in the peridotites with radiogenic Nd isotopic compositions (Fig. 6) can be ascribed to the interaction between asthenospheric melt and peridotites since secondary contamination mentioned above was removed by a combination of leaching and handpicking. The intermineral isotopic disequilibrium, i.e., incomplete diffusive re-equilibration within the xenoliths indicates that the interval between the metasomatic event and sampling by basaltic magmas is relatively short. Equilibrium should be established after 30 Ma on a cm scale of mineral (Jagoutz 1988) based on experimental determination of Sr and Sm diffusion coefficients (1×10^{-15} cm^2/s) in natural cpx at mantle temperature of 1,200°C (Sneeringer et al. 1984). In other words, the event of asthenospheric melt–peridotite interaction possibly occurred recently (shortly before the eruption of host basalts).

The modification of lithospheric mantle by recent asthenospheric melt–peridotite interaction is progressive and comprehensive from the interior to the northern margin of the NCC (Tang et al. 2008). More intensive modification could make the Hannuoba peridotites more radiogenic Nd than those from Yangyuan and Fanshi (Fig. 6). Since the most depleted sample should have low modal cpx content if there was only one ancient depletion event, the observation that most samples having radiogenic Nd isotopic compositions are high in modal cpx contents (11–15%) may indicate that cpx crystallization is related to the melt infiltration (i.e., more isotopic overprint related to the asthenospheric melt coupled with an increase in modal cpx). The cpx separates have more radiogenic Nd and unradiogenic Sr than the coexisting opx, indicating that the cpx could be newly generated or highly modified by the recent asthenospheric melt–peridotite interaction relative to the opx. Thus, the cpx are more susceptible to the asthenospheric melt–peridotite interaction than the opx. This is consistent with the indication based on the Li partitioning between cpx and opx although the time scales of Li and Sr–Nd disequilibrium may be different due to the vastly faster diffusion of Li relative to Sr and Nd.

Origin of Li isotopic fractionation in the peridotites

Diffusion is an important mechanism for the Li isotopic variation in mantle peridotites (Richter et al. 2009). However, the nature of Li diffusion processes, such as the cooling of magmatic systems (Beck et al. 2006; Ionov and Seitz 2008), interaction of peridotites or xenoliths with percolating melts and/or host magmas (Rudnick and Ionov 2007; Magna et al. 2008; Zhang et al. 2010) and recycled melt with low δ^7Li (Nishio et al. 2004; Tang et al. 2007b), is currently disputed although these processes are not mutually exclusive. Given that these processes can

produce isotopic fractionation, it is important to discuss them before considering a possible explanation for our observations.

Redistribution of Li during cooling of magmatic system

Basically most of olivines have relatively low Li contents and normal mantle-like δ^7Li, similar to MORB (Tomascak et al. 2008), whereas the cpx and opx have high Li abundances but low δ^7Li (Fig. 8). The low δ^7Li in the pyroxenes could be generated by diffusion-driven kinetic isotope fractionation due to Li ingress from melt or host magma (e.g., Rudnick and Ionov 2007) and/or from coexisting olivine by subsolidus intermineral Li-redistribution during slow cooling (e.g., Ionov and Seitz 2008). This should be a recent event (shortly before emplacement of the xenolith-bearing magma) because the isotopic disequilibrium between olivine and pyroxenes would rapidly disappear or be obscured due to the fast diffusivity of Li at magmatic temperatures (Rudnick and Ionov 2007). For example, Li equilibration of small (1–2 cm width) veins or melt conduits can be achieved within 10–10^5 years at mantle wedge temperature (Halama et al. 2009).

However, the model of cooling of magmatic systems (e.g., Gallagher and Elliott 2009) cannot sufficiently explain the observations in this study. This model describes Li isotopic fractionation by diffusion during the grain-scale redistribution related to cooling. In this model, cpx may have low δ^7Li, while olivine primarily retains normal mantle-like (or high) δ^7Li due to the faster diffusion of ^{6}Li than ^{7}Li from olivine to cpx during cooling (e.g., Ionov and Seitz 2008). Thus, this model can explain the high δ^7Li in olivine and low δ^7Li in cpx. However, the olivine δ^7Li in a few samples (e.g., −7.9‰ in FS5 and −3.0‰ in FS13), much lower than the normal mantle, is not consistent with the aforementioned model. In addition, the high Li contents (Table 3) and Li partitioning between minerals suggest Li addition possibly by melt infiltration, rather than a simple cooling process.

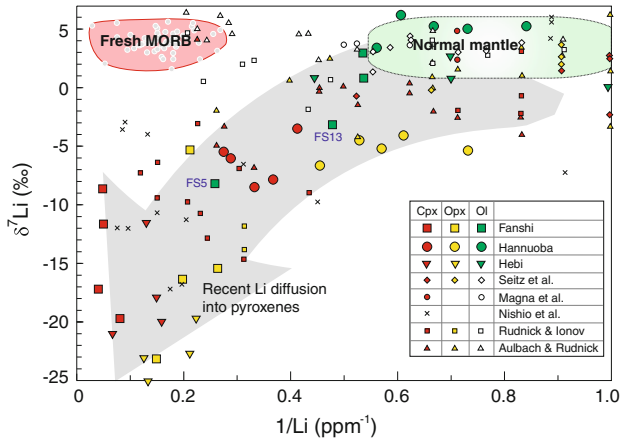

Fig. 8 Variation of δ^7Li with Li concentration for minerals in the studied peridotite xenoliths, compared with published data for fresh MORB (Chan et al. 1992; Tomascak and Langmuir 1999, 2008; Elliott et al. 2006) and peridotites (Nishio et al. 2004; Seitz et al. 2004; Magna et al. 2006; Tang et al. 2007b; Rudnick and Ionov 2007; Aulbach and Rudnick 2009). Gray arrow shows the trend for recent Li diffusion into pyroxenes

Influx of recycled melt with low δ^7Li

Several previous studies suggested the existence of recycled materials with low δ^7Li in the mantle (Zack et al. 2003; Nishio et al. 2004; Tang et al. 2007b). One can assume that the δ^7Li of coexisting olivine should be also low if the low δ^7Li of pyroxenes was the effect of low-δ^7Li melt. However, the olivines in most peridotites have normal mantle-like δ^7Li (Fig. 8), which does not favor this assumption. Moreover, it has been proposed that dehydration can only produce δ^7Li decrease of $\leq$3‰, and the deeply subducted eclogites could be higher in δ^7Li than the mantle (Marschall et al. 2007). This is supported by the high δ^7Li of HIMU lavas (Chan et al. 2009; Vlastélic et al. 2009), which are thought to derive from a mantle source into which oceanic crust has been recycled. Thus, this assumption is short of cogent evidence.

Interaction of peridotites or xenoliths with percolating melts and/or host magmas

Diffusion-driven kinetic Li isotope fractionation during the Li ingress into minerals from percolating melts or host magmas suggests that the Li enrichment occurred shortly before or coincident with the entrainment into the host magmas and the transport of the xenoliths to the surface (Rudnick and Ionov 2007). This model can explain the relatively high δ^7Li in olivine and low δ^7Li in cpx with high Li abundance since Li diffusion into cpx is faster than into olivine (Dohmen et al. 2010). In order to explore models of late-stage Li enrichments by percolating mafic melts, Magna et al. (2008) studied Li abundances and isotopes in three xenoliths containing quenched mafic melts of mantle origin and found slightly higher Li (2.6–4.5 ppm) than normal mantle (*ca* 1–2 ppm) and only moderately fractionated Li isotopes (−3.0 to +2.5‰) in those melt pockets. The results of Magna et al. (2008) cannot well address our observations: (1) much higher Li abundances and larger fractionation of Li isotopes (Table 3) and (2) the low δ^7Li in olivine (−7.9‰) and cpx (−8.4‰) in the sample FS5, showing an approximate intermineral isotopic equilibrium, which may require a bulk ingress of light Li and a relatively long retention time in the mantle. There are two possibilities accountable for the inconsistency between the previous results and our observations: (1) the mechanism of Li

isotopic fractionation (Li behavior) in mantle peridotites and xenoliths is not very clear and (2) present-day observations are fairly limited, for example, only three pockets were analyzed in the previous study. Thus, the actual fractionation of Li isotopes in mantle peridotites or xenoliths may be still highly unconstrained.

Combined effects of diffusive kinetic fractionation during melt/fluid-peridotite interaction and cooling of magmatic system

Based on the aforementioned discussions, our observations may reflect the combined effects of diffusion-driven kinetic fractionation of Li isotopes during melt/fluid-peridotite interactions and the cooling of host magmas. The most likely explanation for the low δ^7Li in the samples FS5 and FS13 is that light Li domains may be existent in the mantle although they cannot persist for extended period of time (Halama et al. 2008; Dohmen et al. 2010). These domains could be produced by diffusion on a large scale of meters because large-scale heterogeneity could survive diffusion of Li isotopes over time scales longer than the small (Vlastélic et al. 2009). Diffusive influx of Li from melt channels into the surrounding lithospheric mantle at depth could produce Li concentration profiles on meter scale, probably similar to the model of alkali diffusion and melt extraction proposed by Lundstrom et al. (2005), who observed that the maximum distance for changes in δ^7Li is around 3 meters. A similar process, Li diffusion from pegmatite into country rock, described by Teng et al. (2006), produced δ^7Li variations to a maximum distance of *ca* 50 m. Therefore, the scale of low-δ^7Li domains caused by diffusion of Li from melt channels into wall rock can be tens of meters. Xenoliths, which represent fragments ripped off from the wall rock of melt channels, will record the bulk enrichment and diffusively fractionated δ^7Li (e.g., low δ^7Li in sample FS5). Other samples may be close enough or far enough from the Li source, so that they show normal mantle values or even higher δ^7Li (see Lundstrom et al. 2005). This explanation is consistent with the recent asthenospheric melt–peridotite interaction suggested by the petrology, trace element and Sr and Nd isotopic characteristics of the peridotites from this region.

A very recent study suggested that the effective diffusion coefficients of many elements (e.g., Li, Ca and Y) in olivine fell within a factor of three of the Mg–Fe interdiffusion coefficient (Qian et al. 2010), in agreement with the results from experiments at higher temperatures that the diffusion rate of Li into olivine is similar to that of the divalent cations (Dohmen et al. 2010; Parkinson et al. 2007; Spandler and O'Neill 2010). Thus, the diffusion coefficient of Li can be similar to that of Sr, indicating that Li, Sr and Nd isotope systems in the peridotites could have been reset by the same event of recently occurred asthenospheric melt/fluid-peridotite interaction.

It should be underlined that the diffusive fractionation of Li isotopes on the grain scale during cooling of the xenoliths, due to temperature-dependent partition coefficient of Li (Coogan et al. 2005; Wunder et al. 2006; Gallagher and Elliott 2009), could have further lowered the δ^7Li in the pyroxenes by Li ingress from host magma and coexisting olivines (subsolidus intermineral Li-redistribution). This probably happened during xenolith entrainment, ascent, eruption and cooling of host magma.

Implication of melt/fluid-peridotite interaction

The transformation of old lithosphere beneath the NCC is not only the large-scale thinning of the lithosphere but also the great change of the lithospheric mantle from highly refractory to fertile in mineral compositions and from high ε_{Sr} and low ε_{Nd} to low ε_{Sr} and high ε_{Nd} in isotopic compositions (Zhang 2005; Menzies et al. 2007; Tang et al. 2008). Because the peridotite xenoliths hosted in the Cenozoic basalts from the eastern NCC have "oceanic-like" geochemical characteristics (fertile in mineral compositions and radiogenic Nd isotopic compositions), they are considered to represent newly accreted lithospheric mantle (Fan et al. 2000; Xu 2001; Ying et al. 2006). One can speculate that if all the "oceanic-like" mantle peridotite xenoliths are newly accreted, they should be young rather than old, which is conflicting with the facts that the Hannuoba peridotites have Proterozoic Re depletion ages (Gao et al. 2002; Zheng et al. 2007; Zhang et al. 2009), and Yangyuan, Fanshi and Hebi peridotites (Fig. 1) have Neoarchean to Paleoproterozoic Re depletion ages (Zheng et al. 2007; Xu et al. 2008a, b). This indicates that not all the peridotitic xenoliths bearing a resemblance to "oceanic-like" mantle are newly accreted and some are still old lithospheric samples. Now the question is what process changed the elemental and isotopic compositions of the old lithospheric mantle?

Asthenosphere–lithosphere and mantle–crust interactions have been used to account for the changes of subcontinental lithospheric mantle beneath ancient cratons (such as Kaapvaal) in the world (Downes 2001; Foley 2008), including the NCC (e.g., Menzies et al. 1993). Coupled with previous studies, the Sr–Nd–Li isotopic disequilibria between the peridotite minerals provide further evidence that the lithospheric mantle beneath the NCC experienced multistage melt/fluid-peridotite interactions. During early stage, the initial melt/fluid-peridotite interaction resulted in unradiogenic Nd isotopic compositions in the modified lithospheric mantle; during later stages, asthenospheric melt/fluid interacted with the old peridotites and led to the great change of the lithospheric mantle (Zhang 2005; Tang et al. 2008; Zhang et al. 2008, 2009), concomitant ε_{Nd} increase. Recent melt/fluid-peridotite interaction may also cause the change of mineral δ^7Li recorded by the peridotite xenoliths.

Recent investigations suggest that melt/fluid-rock interactions may be widely existent in the mantle beneath the whole craton, including the northern (Zhang et al. 2003), the eastern (Zhang 2005; Zhang et al. 2010), the southern (Zheng et al. 2006) and the western (Xu et al. 2005) part of the craton. Therefore, melt/fluid-peridotite interaction could be a key mechanism triggering the compositional change and large-scale thinning of the lithospheric mantle.

Conclusions

The coexisting minerals in the peridotites from the NCC display remarkable Li elemental and Sr–Nd–Li isotopic disequilibria. The cpx have the highest Li contents, followed by opx and olivine, and the mineral Li abundances are significantly higher than the normal mantle. Most olivine δ^7Li are similar to the normal mantle, whereas the δ^7Li of coexisting pyroxenes are very low (−3.3 to −23‰), suggesting recent diffusive ingress of Li into the pyroxenes. Two peridotites have olivine δ^7Li of negative values, much lower than the normal mantle, which may reflect the existence of low δ^7Li domain in the mantle, perhaps generated by meter-scale diffusion of Li during melt/fluid-peridotite interaction.

The ^{143}Nd/^{144}Nd (0.5123–0.5139) and ^{87}Sr/^{86}Sr (0.7018–0.7062) in the cpx and opx separates show a large variation, from DM- to EM1-like compositions. The cpx are lower in ^{87}Sr/^{86}Sr and slightly higher in ^{143}Nd/^{144}Nd than coexisting opx. This Sr–Nd isotopic disequilibrium is more apparent in peridotites with radiogenic Nd isotopic compositions than in those with unradiogenic Nd isotopic compositions. Such an observation suggests a recent interaction between an ancient lithospheric mantle and asthenospheric melt, which transferred the relatively refractory peridotites with highly radiogenic Sr isotopic compositions to the fertile lherzolites with Sr–Nd isotopic compositions approaching the DM end member, although ancient metasomatic event(s) of small volume LREE-enriched melt(s) were required to produce the original mantle with an EM1 composition before the interaction. In the meanwhile, the recent melt/fluid-peridotite interaction may also cause the intermineral Li elemental and isotopic disequilibria.

Collectively, the lithospheric mantle beneath the NCC has been heterogeneously refertilized by multistage melt/fluid-peridotite interactions with the more comprehensive refertilization from the central craton (Hebi area) toward the craton margin (Hannuoba area), which could be a key mechanism producing the transformation of the lithospheric mantle.

Acknowledgments We are very grateful to Moriguti Takuya, Kobayashi Katsura and Akio Makishima for their help in clean lab works to Chie Sakaguchi and Hiroshi Kitagawa for their assistance for Sr–Nd isotopic analysis. We acknowledge the valuable comments by Paul Tomascak, Horst Marschall, Sonja Aulbach, Bjorn Mysen, Ralf Halama and an anonymous reviewer and editorial suggestions of Timothy L. Grove, which helped to improve the different versions of the manuscript. Inspiring discussions with Horst Marschall, Feng Guo and Wei Yang were highly appreciated. This research was financially supported by the Natural Science Foundation of China (90714008, 40773026 and 40534022), the State Key Laboratory of Lithospheric Evolution, Institute of Geology and Geophysics, CAS (0808), and the program of COE-21 designated to the Institute for Study of the Earth's Interior, Okayama University, Japan.

Appendix

See Table 5.

Table 5 Estimated mineral mode (%) and major elemental compositions in the peridotites

Sample	FS5	FS13	FS14	FS19	HB27	HB30	HB80	HB81	D4	D5
Mode										
Olivine	62	66	60	63	70	72	79	73	55	63
Opx	24	21	17	24	27	25	19	24	30	20
Cpx	13	12	8	11	2	1	1	1	13	15
Spinel	1	1	5	2	1	2	1	2	2	2
SiO_2	45.67	44.85	43.30	45.33	44.15	43.96	43.56	43.66	45.93	45.05
TiO_2	0.07	0.09	0.03	0.08	0.04	0.01	0.02	0.02	0.10	0.12
Al_2O_3	2.16	2.16	3.67	2.39	1.15	1.37	0.75	0.96	3.29	2.67
Cr_2O_3	0.32	0.28	0.90	0.53	0.70	0.94	0.62	1.02	0.39	0.57
MgO	40.22	41.99	42.88	41.23	44.89	45.42	46.99	45.91	38.51	40.09
CaO	2.69	2.67	1.77	2.43	0.67	0.42	0.42	0.39	2.87	3.22
MnO	0.12	0.13	0.12	0.14	0.12	0.09	0.12	0.10	0.10	0.12
FeO	8.14	8.30	7.57	7.59	6.60	7.29	7.24	7.24	7.92	7.56
NiO	0.23	0.27	0.36	0.27	0.28	0.28	0.29	0.30	0.24	0.25
Na_2O	0.20	0.21	0.11	0.17	0.04	0.08	0.01	0.03	0.25	0.27
Total	99.8	100.9	100.7	100.2	99.6	99.9	98.6	99.6	99.6	99.9
Mg#	89.9	90.1	91.1	90.7	92.3	91.9	92.2	92.1	89.7	90.5

Data for D4 and D5 are from Tang et al. (2007a)

References

Agostini S, Ryan JG, Tonarini S, Innocenti F (2008) Drying and dying of a subducted slab: coupled Li and B isotope variations in Western Anatolia Cenozoic Volcanism. Earth Planet Sci Lett 272:139–147

Anders E, Grevesse N (1989) Abundances of the elements: meteoritic and solar. Geochim Cosmochim Acta 53:197–214

Aulbach S, Rudnick RL (2009) Origins of non-equilibrium lithium isotope fractionation in xenolithic peridotite minerals: examples from Tanzania. Chem Geol 258:17–27

Aulbach S, Rudnick RL, McDonough WF (2008) Li–Sr–Nd isotope signatures of the plume and cratonic lithospheric mantle beneath the margin of the rifted Tanzanian craton (Labait). Contrib Mineral Petrol 155:79–92

Basu A, Murthy VR (1976) Sr isotopes and trace elements in spinel lherzolite xenoliths in basalts, San Quintin, Baja California. EOS Trans Am Geophys Union 57:354 (abstract)

Beck P, Chaussidon M, Barrat JA, Gillet P, Bohn M (2006) Diffusion induced Li isotopic fractionation during the cooling of magmatic rocks: the case of pyroxene phenocrysts from nakhlite meteorites. Geochim Cosmochim Acta 70:4813–4825

Bodinier JL, Menzies MA, Shimizu N, Frey FA, McPherson E (2004) Silicate, hydrous and carbonate metasomatism at Lherz, France: contemporaneous derivatives of silicate melt-harzburgite reaction. J Petrol 45:299–320

Boyd FR (1989) Compositional distinction between oceanic and cratonic lithosphere. Earth Planet Sci Lett 96:15–26

Brenan JM, Ryerson FJ, Shaw HF (1998) The role of aqueous fluids in the slab-to-mantle transfer of boron, beryllium, and lithium during subduction: experiments and models. Geochim Cosmochim Acta 62:3337–3347

Burwell ADM (1975) Rb-Sr isotope geochemistry of lherzolites and their constituent minerals from Victoria, Australia. Earth Planet Sci Lett 28:69–78

Carlson RW, Irving AJ, Schulze DJ, Hearn BC (2004) Timing of Precambrian melt depletion and Phanerozoic refertilization events in the lithospheric mantle of the Wyoming Craton and adjacent Central Plains Orogen. Lithos 77:453–472

Chan LH, Edmond JM, Thompson G, Gillis K (1992) Lithium isotopic composition of submarine basalts: implications for the lithium cycle in the oceans. Earth Planet Sci Lett 108:151–160

Chan LH, Lassiter JC, Hauri EH, Hart SR, Blusztajn J (2009) Lithium isotope systematics of lavas from the Cook-Austral Islands: Constraints on the origin of HIMU mantle. Earth Planet Sci Lett 277:433–442

Chen SH, O'Reilly SY, Zhou XH, Griffin WL, Zhang GH, Sun M, Feng JL, Zhang M (2001) Thermal and petrological structure of the lithosphere beneath Hannuoba, Sino-Korean Craton, China: evidence from xenoliths. Lithos 56:267–301

Chi JS, Lu FX (1996) Kimberlites on the North China Craton and features of Paleozoic lithospheric mantle. China Science Press, Beijing (in Chinese)

Coogan LA, Kasemann SA, Chakraborty S (2005) Rates of hydrothermal cooling of new oceanic upper crust derived from lithium-geospeedometry. Earth Planet Sci Lett 240:415–424

Dobbs PN, Duncan DJ, Hu S, Shee SR, Colgan E, Brown MA, Smith CB, Allsopp HL (1994) The geology of the Mengyin kimberlites, Shandong, China. In: Meyer HOA, Leonardos OH (eds) Diamonds: characterization, genesis and exploration, Proceedings of 5th international Kimb conference 1. CPRM, Brasilia, pp 106–115

Dohmen R, Kasemann SA, Coogan L, Chakraborty S (2010) Diffusion of Li in olivine. Part I: experimental observations and a multi species diffusion model. Geochim Cosmochim Acta 74:274–292

Downes H (2001) Formation and modification of the shallow subcontinental lithospheric mantle: a review of geochemical evidence from ultramafic xenolith suites and tectonically emplaced ultramafic massifs of western and central Europe. J Petrol 42:233–250

Elliott T, Thomas A, Jeffcoate A, Niu YL (2006) Lithium isotope evidence for subduction-enriched mantle in the source of mid-ocean-ridge basalts. Nature 443:565–568

Fan QC, Hooper PR (1989) The mineral chemistry of ultramafic xenoliths of Eastern China-implications for upper mantle composition and the paleogeotherms. J Petrol 30:1117–1158

Fan WM, Menzies MA (1992) Destruction of aged lower lithosphere and accretion of asthenosphere mantle beneath eastern China. Geotectonica et Metallogenia 16:171–180

Fan WM, Zhang HF, Baker J, Jarvis KE, Mason PRD, Menzies MA (2000) On and off the north China craton: Where is the Archaean keel? J Petrol 41:933–950

Foley SF (2008) Rejuvenation and erosion of the cratonic lithosphere. Nat Geosci 1:503–510

Gallagher K, Elliott T (2009) Fractionation of lithium isotopes in magmatic systems as a natural consequence of cooling. Earth Planet Sci Lett 278:286–296

Gao S, Rudnick RL, Carlson RW, McDonough WF, Liu YS (2002) Re–Os evidence for replacement of ancient mantle lithosphere beneath the North China craton. Earth Planet Sci Lett 198:307–322

Griffin WL, O'Reilly SY, Ryan CG (1992) Composition and thermal structure of the lithosphere beneath South Africa, Siberia and China: proton microprobe studies. In: International symposium on cenozoic volcanic rocks and deep-seated xenoliths of China and its environs, pp 65–66

Griffin WL, O'Reilly SY, Abe N, Aulbach S, Davies RM, Pearson NJ, Doyle BJ, Kivi K (2003) The origin and evolution of Archean lithospheric mantle. Precam Res 127:19–41

Halama R, McDonough WF, Rudnick RL, Bell K (2008) Tracking the lithium isotopic evolution of the mantle using carbonatites. Earth Planet Sci Lett 265:726–742

Halama R, Savov IP, Rudnick RL, McDonough WF (2009) Insights into Li and Li isotope cycling and sub-arc metasomatism from veined mantle xenoliths, Kamchatka. Contrib Miner Petrol 158:197–222

He GZ (1987) Mantle xenoliths from kimberlites in China. In: Nixon PH (ed) Mantle xenoliths. Wiley, Chichester, pp 182–185

Herzberg CT (1993) Lithosphere peridotites of the Kaapvaal Craton. Earth Planet Sci Lett 120:13–29

Huh Y, Chan LH, Zhang L, Edmond JM (1998) Lithium and its isotopes in major world rivers: implications for weathering and the oceanic budget. Geochim Cosmochim Acta 62:2039–2051

Ionov DA, Seitz HM (2008) Lithium abundances and isotopic compositions in mantle xenoliths from subduction and intra-plate settings: mantle sources vs. eruption histories. Earth Planet Sci Lett 266:316–331

Ionov DA, Mukasa SB, Bodinier JL (2002) Sr–Nd–Pb isotopic compositions of peridotite xenoliths from Spitsbergen: numerical modelling indicates Sr–Nd decoupling in the mantle by melt percolation metasomatism. J Petrol 43:2261–2278

Jagoutz E (1988) Nd and Sr systematics in an eclogite xenolith from Tanzania: evidence for frozen mineral equilibria in the continental lithosphere. Geochim Cosmochim Acta 52:1285–1293

Jagoutz E, Carlson RW, Lugmair GW (1980) Equilibrated Nd-unequilibrated Sr isotopes in mantle xenoliths. Nature 286: 708–710

Jeffcoate AB, Elliott T, Kasemann SA, Ionov D, Cooper K, Brooker R (2007) Li isotope fractionation in peridotites and mafic melts. Geochim Cosmochim Acta 71:202–218

Kaliwoda M, Ludwig T, Altherr R (2008) A new SIMS study of Li, Be, B and δ7Li in mantle xenoliths from Harrat Uwayrid (Saudi Arabia). Lithos 106:261–279

Kobayashi K, Tanaka R, Moriguti T, Shimizu K, Nakamura E (2004) Lithium, boron, and lead isotope systematics of glass inclusions in olivines from Hawaiian lavas: evidence for recycled components in the Hawaiian plume. Chem Geol 212:143–161

Košler J, Magna T, Mlcoch B, Mixa P, Nýlt D, Holub FV (2009) Combined Sr, Nd, Pb and Li isotope geochemistry of alkaline lavas from northern James Ross Island (Antarctic Peninsula) and implications for back-arc magma formation. Chem Geol 258:207–218

Kushiro I (2001) Partial melting experiments on peridotite and origin of mid-ocean ridge basalt. Annu Rev Earth Planet Sci 29:71–107

Lee CTA, Oka M, Luffi P, Agranier A (2008) Internal distribution of Li and B in serpentinites from the Feather River Ophiolite, California, based on laser ablation inductively coupled plasma mass spectrometry. Geochem Geophys Geosyst 9. doi:12010.11029/12008GC002078

Liu DY, Nutman AP, Compston W, Wu JS, Shen QH (1992) Remnants of 3800 Ma crust in the Chinese part of the Sino-Korean craton. Geology 20:339–342

Lundstrom CC, Chaussidon M, Hsui AT, Kelemen P, Zimmerman M (2005) Observations of Li isotopic variations in the Trinity Ophiolite: Evidence for isotopic fractionation by diffusion during mantle melting. Geochim Cosmochim Acta 69:735–751

Ma JL, Xu YG (2006) Old EM1-type enriched mantle under the middle North China Craton as indicated by Sr and Nd isotopes of mantle xenoliths from Yangyuan, Hebei Province. Chin Sci Bullet 51:1343–1349

Magna T, Wiechert U, Halliday AN (2006) New constraints on the lithium isotope compositions of the Moon and terrestrial planets. Earth Planet Sci Lett 243:336–353

Magna T, Ionov DA, Oberli F, Wiechert U (2008) Links between mantle metasomatism and lithium isotopes: Evidence from glass-bearing and cryptically metasomatized xenoliths from Mongolia. Earth Planet Sci Lett 276:214–222

Makishima A, Nakamura E (2006) Determination of major, minor and trace elements in silicate samples by ICP-QMS and ICP-SFMS applying isotope dilution-internal standardisation (ID-IS and multi-stage internal standardisation). Geostand Geoanal Res 30:245–271

Marks MAW, Rudnick RL, McCammon C, Vennemann T, Markl G (2007) Arrested kinetic Li isotope fractionation at the margin of the llimaussaq complex, South Greenland: Evidence for open-system processes during final cooling of peralkaline igneous rocks. Chem Geol 246:207–230

Marschall HR, Pogge von Strandmann PAE, Seitz HM, Elliott T, Niu Y (2007) The lithium isotopic composition of orogenic eclogites and deep subducted slabs. Earth Planet Sci Lett 262:563–580

McDonough WF, McCulloch MT (1987) The southeast Australian lithospheric mantle: isotopic and geochemical constraints on its growth and evolution. Earth Planet Sci Lett 86:327–340

McDonough WF, Sun SS (1995) The composition of the earth. Chem Geol 120:223–253

Menzies MM, Murthy VR (1978) Strontium isotope geochemistry of alpine tectonite lherzolites: data compatible with a mantle origin. Earth Planet Sci Lett 38:346–354

Menzies M, Murthy VR (1980) Enriched mantle: Nd and Sr isotopes in diopsides from kimberlite nodules. Nature 283:634–636

Menzies MA, Fan WM, Zhang M (1993) Palaeozoic and Cenozoic lithoprobes and the loss of >120 km of Archaean lithosphere, Sino-Korean craton, China. In: Prichard HM, Alabaster T, Harris NBW, Neary CR (eds) Magmatic processes and plate tectonics. Geol Soc London, vol 76, pp 71–81

Menzies M, Xu YG, Zhang HF, Fan WM (2007) Integration of geology, geophysics and geochemistry: a key to understanding the North China Craton. Lithos 96:1–21

Meyer HOA, Waldman MA, Garwood BL (1994) Mantle xenoliths from kimberlite near Kirkland Lake, Ontario. Can Miner 32:295–306

Moriguti T, Nakamura E (1998) High-yield lithium separation and the precise isotopic analysis for natural rock and aqueous samples. Chem Geol 145:91–104

Moriguti T, Makishima A, Nakamura E (2004) Determination of Lithium contents in silicates by isotope dilution ICP-MS and its evaluation by isotope dilution thermal ionisation mass spectrometry. Geostand Geoanal Res 28:371–382

Nakamura E, Makishima A, Moriguti T, Kobayashi K, Sakaguchi C, Yokoyma T, Tanaka R, Kuritani T, Takei H (2003) Comprehensive geochemical analyses of small amounts (<100 mg) of extraterrestrial samples for the analytical competition related to the sample return mission MUSES-C. In: Kushiro I, Fujiwara A, Yano H (eds) Asteroidal sample preliminary examination team, Inst Space and Astron Sci Report SP, vol 16, pp 49–101

Navon O, Stolper E (1987) Geochemical consequence of melt percolation-the upper mantle as a chromatographic column. J Geol 95:285–307

Nishio Y, Shun'ichi N, Yamamoto J, Sumino H, Matsumoto T, Prikhod'ko VS, Arai S (2004) Lithium isotopic systematics of the mantle-derived ultramafic xenoliths: implications for EM1 origin. Earth Planet Sci Lett 217:245–261

Ottolini L, Laporte D, Raffone N, Devidal JL, Le FB (2009) New experimental determination of Li and B partition coefficients during upper mantle partial melting. Contrib Miner Petrol 157:313–325

Parkinson IJ, Hammond SJ, James RH, Rogers NW (2007) High-temperature lithium isotope fractionation: insights from lithium isotope diffusion in magmatic systems. Earth Planet Sci Lett 257:609–621

Paul DK (1971) Strontium isotope studies on ultramafic inclusions from Dreiser Weiher, Eifel, Germany. Contrib Miner Petrol 34:22–28

Penniston-Dorland SC, Sorensen SS, Ash RD, Khadke SV (2010) Lithium isotopes as a tracer of fluids in a subduction zone mélange: Franciscan Complex, CA. Earth Planet Sci Lett 292:181–190

Qian Q, O'Neill HSC, Hermann J (2010) Comparative diffusion coefficients of major and trace elements in olivine at 950°C from a xenocryst included in dioritic magma. Geology 38:331–334

Richardson SH, Erlank AJ, Hart SR (1985) Kimberlite-borne garnet peridotite xenoliths from old enriched subcontinental lithosphere. Earth Planet Sci Lett 75:116–128

Richter FM, Davis AM, Depaolo DJ, Watson EB (2003) Isotope fractionation by chemical diffusion between molten basalts and rhyolite. Geochim Cosmochim Acta 67:3905–3923

Richter FM, Dauphas N, Teng FZ (2009) Non-traditional fractionation of non-traditional isotopes: evaporation, chemical diffusion and Soret diffusion. Chem Geol 258:92–103

Rudnick RL, Ionov DA (2007) Lithium elemental and isotopic disequilibrium in minerals from peridotite xenoliths from far-east Russia: product of recent melt/fluid-rock reaction. Earth Planet Sci Lett 256:278–293

Rudnick RL, Gao S, Ling WL, Liu YS, McDonough WF (2004) Petrology and geochemistry of spinel peridotite xenoliths from Hannuoba and Qixia, North China Craton. Lithos 77:609–637

Seitz HM, Woodland AB (2000) The distribution of lithium in peridotitic and pyroxenitic mantle lithologies—an indicator of magmatic and metasomatic processes. Chem Geol 166:47–64

Seitz HM, Brey GP, Lahaye Y, Durali S, Weyer S (2004) Lithium isotopic signatures of peridotite xenoliths and isotopic fractionation at high temperature between olivine and pyroxenes. Chem Geol 212:163–177

Simon NSC, Carlson RW, Pearson DG, Davies GR (2007) The origin and evolution of the Kaapvaal cratonic lithospheric mantle. J Petrol 48:589–625

Sneeringer M, Hart SR, Shimizu N (1984) Strontium and samarium diffusion in diopside. Geochim Cosmochim Acta 48:1589–1608

Song Y, Frey FA (1989) Geochemistry of peridotite xenoliths in basalt from Hannuoba, eastern China: implications for subcontinental mantle heterogeneity. Geochim Cosmochim Acta 53:97–113

Spandler C, O'Neill H (2010) Diffusion and partition coefficients of minor and trace elements in San Carlos olivine at 1,300°C with some geochemical implications. Contrib Mineral Petrol. doi:10.1007/s00410-00009-00456-00418

Stosch HG, Lugmair GW, Kovalenko VI (1986) Spinel peridotite xenoliths from the Tariat Depression, Mongolia. II: geochemistry and Nd and Sr isotopic composition and their implications for the evolution of the subcontinental lithosphere. Geochim Cosmochim Acta 50:2601–2614

Tang YJ, Zhang HF, Ying JF (2006) Asthenosphere-lithospheric mantle interaction in an extensional regime: implication from the geochemistry of Cenozoic basalts from Taihang Mountains, North China Craton. Chem Geol 233:309–327

Tang YJ, Zhang HF, Ying JF (2007a) Review of the lithium isotope system as a geochemical tracer. Int Geol Rev 49:374–388

Tang YJ, Zhang HF, Nakamura E, Moriguti T, Kobayashi K, Ying JF (2007b) Lithium isotopic systematics of peridotite xenoliths from Hannuoba, North China Craton: implications for melt-rock interaction in the considerably thinned lithospheric mantle. Geochim Cosmochim Acta 71:4327–4341

Tang YJ, Zhang HF, Ying JF, Zhang J, Liu XM (2008) Refertilization of ancient lithospheric mantle beneath the central North China Craton: evidence from petrology and geochemistry of peridotite xenoliths. Lithos 101:435–452

Tatsumoto M, Basu AR, Huang WK, Wang JW, Xie GH (1992) Sr, Nd, and Pb isotopes of ultramafic xenoliths in volcanic rocks of eastern China: enriched components EMI and EMII in subcontinental lithosphere. Earth Planet Sci Lett 113:107–128

Teng FZ, McDonough WF, Rudnick RL, Walker RJ (2006) Diffusion-driven extreme lithium isotopic fractionation in country rocks of the Tin Mountain pegmatite. Earth Planet Sci Lett 243:701–710

Tomascak PB (2004) Developments in the understanding and application of lithium isotopes in the earth and planetary sciences. In: Johnson CM, Beard BI, Albarede F (eds) Geochemistry of non-traditional stable isotope: Reviews in Mineralogy and Geochemistry. Mineral Soc Am, vol 55, pp 153–195

Tomascak PB, Langmuir CH (1999) Lithium isotope variability in MORB. Eos Trans AGU 80:F1086–F1087

Tomascak PB, Carlson RW, Shirey SB (1999) Accurate and precise determination of Li isotopic compositions by multi-collector sector ICP-MS. Chem Geol 158:145–154

Tomascak PB, Ryan JG, Defant MJ (2000) Lithium isotope evidence for light element decoupling in the Panama subarc mantle. Geology 28:507–510

Tomascak PB, Langmuir CH, le Roux PJ, Shirey SB (2008) Lithium isotopes in global mid-ocean ridge basalts. Geochim Cosmochim Acta 72:1626–1637

Vlastélic I, Koga K, Chauvel C, Jacques G, Télouk P (2009) Survival of lithium isotopic heterogeneities in the mantle supported by HIMU-lavas from Rurutu Island, Austral Chain. Earth Planet Sci Lett 286:456–466

Wagner C, Deloule E (2007) Behaviour of Li and its isotopes during metasomatism of French Massif Central lherzolites. Geochim Cosmochim Acta 71:4279–4296

Walter M (1998) Melting of garnet peridotite and the origin of komatiite and depleted lithosphere. J Petrol 39:29–60

Wang YJ, Fan WM, Zhang HF, Peng TP (2006) Early Cretaceous gabbroic rocks from the Taihang Mountains: implications for a paleosubduction-related lithospheric mantle beneath the central North China Craton. Lithos 86:281–302

Woodland AB, Seitz HM, Yaxley GM (2004) Varying behaviour of Li in metasomatised spinel peridotite xenoliths from western Victoria, Australia. Lithos 75:55–66

Wunder B, Meixner A, Romer RL, Heinrich W (2006) Temperature-dependent isotopic fractionation of lithium between clinopyroxene and high-pressure hydrous fluids. Contrib Mineral Petrol 151:112–120

Xu YG (2001) Thermo-tectonic destruction of the Archean lithospheric keel beneath the Sino-Korean Craton in China: Evidence, timing and mechanism. Phys Chem Earth (A) 26:747–757

Xu X, O'Reilly SY, Griffin WL, Zhou X, Huang X (1998a) The nature of the Cenozoic lithosphere of Nushan, eastern China. In: Flower MFJ, Chung SL, Lo CH, Lee TY (eds) Mantle dynamics and plate interactions in East Asia. Geodynamics Series 27, AGU, Washington, pp 167–196

Xu YG, Menzies MA, Bodinier JL, Bedini RM, Vroon P, Mercier JCC (1998b) Melt percolation and reaction atop a plume: evidence from the poikiloblastic peridotite xenoliths from Boree (Massif Central, France). Contrib Mineral Petrol 132:65–84

Xu YG, Ma JL, Frey FA, Feigenson MD, Liu JF (2005) Role of lithosphere-asthenosphere interaction in the genesis of Quaternary alkali and tholeiitic basalts from Datong, western North China Craton. Chem Geol 224:247–271

Xu XS, Griffin WL, O'Reilly SY, Pearson NJ, Geng HY, Zheng JP (2008a) Re–Os isotope of sulfides in mantle xenoliths from eastern China: progressive modification of lithospheric mantle. Lithos 102:43–64

Xu YG, Blusztajn J, Ma JL, Suzuki K, Liu JF, Hart SR (2008b) Late Archean to early Proterozoic lithospheric mantle beneath the western North China craton: Sr-Nd-Os isotopes of peridotite xenoliths from Yangyuan and Fansi. Lithos 102:25–42

Ying JF, Zhang HF, Kita N, Morishita Y, Shimoda G (2006) Nature and evolution of Late Cretaceous lithospheric mantle beneath the eastern North China Craton: Constraints from petrology and geochemistry of peridotitic xenoliths from Jünan, Shandong Province, China. Earth Planet Sci Lett 244:622–638

Yoshikawa M, Nakamura E (1993) Precise isotopic determination of trace amounts of Sr in magnesium-rich samples. J Jpn Soc Miner Petrol Econ Geol 88:548–561

Zack T, Tomascak PB, Rudnick RL, Dalpé C, McDonough WF (2003) Extremely light Li in orogenic eclogites: the role of isotope fractionation during dehydration in subducted oceanic crust. Earth Planet Sci Lett 208:279–290

Zhang HF (2005) Transformation of lithospheric mantle through peridotite-melt reaction: a case of Sino-Korean craton. Earth Planet Sci Lett 237:768–780

Zhang P, Hu S, Wan G (1989) A review of the geology of some kimberlites in China. Geol Soc Spec Publ Aust 14:392–400

Zhang HF, Sun M, Zhou XH, Fan WM, Yin JF (2002) Mesozoic lithosphere destruction beneath the North China Craton: evidence from major, trace element, and Sr-Nd-Pb isotope studies of Fangcheng basalts. Contrib Miner Petrol 144:241–253

Zhang HF, Sun M, Zhou XH, Zhou MF, Fan WM, Zheng JP (2003) Secular evolution of the lithosphere beneath the eastern North China Craton: evidence from Mesozoic basalts and high-Mg andesites. Geochim Cosmochim Acta 67:4373–4387

Zhang HF, Sun M, Zhou MF, Fan WM, Zhou XH, Zhai MG (2004) Highly heterogeneous late Mesozoic lithospheric mantle beneath the north China Craton: evidence from Sr–Nd–Pb isotopic systematics of mafic igneous rocks. Geol Mag 141:55–62

Zhang HF, Nakamura E, Kobayashi K, Zhang J, Ying JF, Tang YJ, Niu LF (2007) Transformation of subcontinental lithospheric mantle through deformation-enhanced peridotite-melt reaction: evidence from a highly fertile mantle xenolith from the North China craton. Int Geol Rev 49:658–679

Zhang HF, Goldstein S, Zhou XH, Sun M, Zheng JP, Cai Y (2008) Evolution of subcontinental lithospheric mantle beneath eastern China: Re–Os isotopic evidence from mantle xenoliths in Paleozoic kimberlites and Mesozoic basalts. Contrib Miner Petrol 155:271–293

Zhang HF, Goldstein SL, Zhou XH, Sun M, Cai Y (2009) Comprehensive refertilization of lithospheric mantle beneath the North China Craton: further Os–Sr–Nd isotopic constraints. J Geol Soc Lond 166:249–259

Zhang HF, Deloule E, Tang YJ, Ying JF (2010) Melt/rock interaction in remains of refertilized Archean lithospheric mantle in Jiaodong Peninsula, North China Craton: Li isotopic evidence. Contrib Miner Petrol 160:261–277

Zhao GC, Wilde SA, Sun M, Li S, Li X, Zhang J (2008) SHRIMP U–Pb zircon ages of granitoid rocks in the Lüliang Complex: Implications for the accretion and evolution of the Trans-North China Orogen. Precam Res 160:213–226

Zhao X, Zhang H, Zhu X, Tang S, Tang Y (2010) Iron isotope variations in spinel peridotite xenoliths from North China Craton: implications for mantle metasomatism. Contrib Miner Petrol doi:10.1007/s00410-009-0461-y

Zheng JP, O'Reilly SY, Griffin W, Lu FX, Zhang M, Pearson N (2001) Relict refractory mantle beneath the eastern North China block: significance for lithosphere evolution. Lithos 57:43–66

Zheng JP, Griffin WL, O'Reilly SY, Zhang M, Pearson N (2006) Zircons in mantle xenoliths record the Triassic Yangtze-North China continental collision. Earth Planet Sci Lett 247:130–142

Zheng JP, Griffin WL, O'Reilly SY, Yu CM, Zhang HF, Pearson N, Zhang M (2007) Mechanism and timing of lithospheric modification and replacement beneath the eastern North China Craton: peridotitic xenoliths from the 100 Ma Fuxin basalts and a regional synthesis. Geochim Cosmochim Acta 71:5203–5225

Zindler A, Hart SR (1986) Chemical geodynamics. Annu Rev Earth Planet Sci 14:493–571

Zindler A, Jagoutz E (1988) Mantle cryptology. Geochim Cosmochim Acta 52:319–333